Surface Composition of a Highly Active Pt3Y Alloy Catalyst for Application in Low Temperature Fuel Cells

(article starts on next page)

Surface Composition of a Highly Active Pt₃Y Alloy Catalyst for Application in Low Temperature Fuel Cells▲

R. Brown[1]*, M. Vorokhta[2], T. Skála[2], I. Khalakhan[2], N. Lindahl[1], B. Eriksson[3],
C. Lagergren[3], I. Matolínová[2], V. Matolín[2], B. Wickman[1]*

[1] Chemical Physics, Department of Physics, Chalmers University of Technology, 41296 Gothenburg, Sweden
[2] Department of Surface and PlasmaScience, Faculty of Mathematics and Physics, Charles University, V Holešovičách 2, 18000 Prague 8, Czech Republic
[3] Applied Electrochemistry, Department of Chemical Engineering, KTH Royal Institute of Technology, Stockholm, 10044 Stockholm, Sweden

Abstract

Currently, platinum is the most widely used catalyst for low temperature proton exchange membrane fuel cells (PEMFC). However, the kinetics at the cathode are slow, and the price of platinum is high. To improve oxygen reduction reaction (ORR) kinetics at the cathode, platinum can be alloyed with rare earth elements, such as yttrium. We report that Pt₃Y has the potential to be over 2 times more active for the ORR compared with Pt inside a real fuel cell. We present detailed photoemission analysis into the nature of the sputtered catalyst surface, using synchrotron radiation photoelectron spectroscopy (SRPES) to examine if surface adsorbates or impuri-

ties are present and can be removed. Pretreatment removes most of the yttrium oxide in the surface leaving behind a Pt overlayer which is only a few monolayers thick. Evidence of a substochiometric oxide peak in the Y 3d core level is presented, this oxide extends into the surface even after Ar⁺ sputter cleaning in-situ. This information will aid the development of new highly active nanocatalysts for employment in real fuel cell electrodes.

Keywords: Alloys, Electrocatalysis, Oxygen Reduction Reaction, Photoelectron Spectroscopy, Platinum, Proton Exchange Membrane Fuel Cells, Rare Earths, Thin Films

1 Introduction

Platinum is the best sole metal for the oxygen reduction reaction (ORR) in low temperature proton exchange membrane fuel cells (PEMFC). However, it is an expensive and scarce material. In order for this kind of fuel cell to become more widespread in society, the cost of a fuel cell must be reduced. One important factor to achieve cheaper PEMFCs is to reduce the amount of platinum in the catalyst layer. Alloys of platinum and rare earth metals have been investigated for the ORR in order to reduce the cost of the catalyst layer [1–4]. These alloys reduce the

amount of platinum required and increase the catalyst activity above that of pure platinum. In fact, Pt₃Y in particular, has been shown to have over 10 times the activity of pure Pt [5–8]. These alloys exhibit increased activity, because a protective, strained and highly active overlayer of pure platinum forms on their surface when treated in acid solution [3, 8, 9].

Initial studies into Pt₃Y focused on single crystalline or bulk materials in liquid half cell setups, which does not directly translate to fuel cell conditions [8–13]. Sputter deposition of

---

[*] Corresponding authors, bjorn.wickman@chalmers.se; brown@chalmers.se

---

the alloy catalyst, in thin film form, provides a simple and effective method to study its activitiy and behavior in real fuel cell conditions. So far, measurements have shown that sputtered Pt₃Y films are just as highly active as bulk alloy [5, 7], so they make a good model system with which to test surface and catalytic properties. Our studies on fuel cell measurements of thin film Pt₃Y show an improved activity compared to pure platinum [6]. However, there are some differences in the activities achieved in literature, depending on the measurement technique and sample preparation [5–7, 10].

With platinum rare earth alloys, the highly active overlayer extends slightly beyond the surface and is affected by the bulk alloy material underneath. In order to understand what influences the activity of the catalyst, is it important to be able to characterize the overlayer in detail, examining the surface compostion.

X-ray photoelectron spectroscopy (XPS), or more generally photoelectron spectroscopy (PES), is commonly used to probe the surface of catalyst materials to investigate its composition. It can provide details of how impurities, oxides and adsorbates are present and bonded in the surface of a catalyst. All of these will affect the resulting activity.

Synchrotron radiation photoelectron spectroscopy (SRPES) provides much higher resolution and higher surface sensitivity than non-monochromated XPS. Photoelectrons are collected from different depths, due to variation of the incoming photon energy. Low concentrations of yttrium and impurites are easily picked up at the lowest photon energies. There are also complexities with this technique, however the gain in surface sensitivity is beneficial for examining the platinum overlayer. In this work, SRPES was used to investigate three important components of the catalytically activity of Pt₃Y: (i) impurities that could affect the performance, (ii) the composition of the platinum overlayer, and (iii) subsurface substochiometric oxide [14]. To observe these three components, SRPES spectra were taken before and after acid treatment. Argon ion sputtering was used to remove surface adsorbates and the top of the overlayer, in order to see how much oxide remained on the surface.

The films lose Y_2O_3 during acid treatment as the Pt overlayer forms. However, not all oxygen is removed during this process as some substochiometric oxide (Y–O) and Y_2O_3 remains. Sputter cleaning removed surface adsorbates and Y_2O_3 but also may have pushed oxygen further into the film. The origin of the Y–O doublet is not completely understood, it could come from *ex situ* oxidation or from the sputter deposition process itself. Regardless, the Pt₃Y films behave as expected in electrochemical characterization and have a significant increase in activity compared to Pt. We expect that complete removal of Y–O will further increase the activity of Pt₃Y.

2 Experimental

2.1 Fuel Cell Measurement

The fuel cell measurement has been described previously [6, 15]. Firstly, the membrane electrode assembly (MEA) was assembled. A circular piece of gas diffusion layer (GDL, Carbel CL) with the 60 nm thick Pt₃Y or Pt sputter deposited catalyst layer was punched with area of 0.95 cm² for use as the cathode. The approximate mass loadings for the samples were 129 μg cm⁻² for Pt, and 99.7 μg cm⁻² for Pt₃Y. The GDL supported catalyst was then immersed in 0.1M HClO₄ three times for 10 min, followed by washing with MilliQ water five times, then left to dry for 30 min. To reduce the effects of hydrogen crossover a double-MEA approach was utilized [6]. A commercial GORE PRIMEA® MEA (anode/cathode loading of 0.1/0.4 mg_Pt cm⁻²) was used as an anode, and a Nafion 212 membrane (thickness 17 μm) was used to isolate the MEA platinum from the catalyst GDL. A 3.14 cm² punched piece of commercial GDL (Carbel CL) was used to complete the cell. Prior to measurement, the MEA was pressed within the cell with a clamping pressure of 12 bar and temperature of 80 °C for 30 s.

All fuel cell measurements were performed with an in-house developed single cell [16]. All activity measurements were performed with a cell temperature of 80 °C, with 100% relative humidity (RH) and a back pressure of 1.5×10^5 Pa (1 bar). For all measurements, 5% H_2 with Ar balance (flow rates of 90 ml min⁻¹) was used at the anode to reduce crossover effects. All measures values refer to the reversible hydrogen electrode (RHE) and they have all been adjusted for the change in potential, due to the lowered partial pressure of H_2. Measurements were performed with a PAR 273A potentiostat.

Prior to electrochemical characterization the MEA's were activated at 80 °C by cycling in 5% H_2 in Ar and O_2 (flow rate of 90 ml min⁻¹) between the potentials of 0.9 and 0.6 V with a sweep rate of 20 mV s⁻¹ for 2,000 cycles. Polarization curves were taken by sweeping between 0.9 and 0.3 V at a rate of 20 mV s⁻¹. This sweep rate was used to increase the signal to noise ratio as the samples had low Pt loading. The cell was then cooled to 30 °C under nitrogen flow overnight. Cyclic voltammetry was then performed between 0.1 and 1.2 V at a rate of 200 mV s⁻¹. CO stripping was performed to obtain the electrochemically active surface area, more details can be found in the supporting information. A baseline was recorded followed by a potential hold at 0.15 V where the working electrode inlet gas was switched to 2% CO in Ar for 2 min. To ensure that no unreacted CO remained, the working electrode gas was switched back to N_2 for 5 min before stripping.

2.2 Sputter Deposition

Thin films of pure Pt and Pt₃Y were deposited using single target (99.99% purity Pt₃Y, Goodfellow; 99.99% purity Pt, Williams Advanced Materials) DC magnetron sputtering in a Nordiko 2000 sputter coater onto glassy carbon disks (Sigradur G, HTW Gmbh) and porous gas diffusion layers (Carbel CL). The base pressure of the sputtering system was lower than 1.0×10^{-4} Pa and sputtering was performed in 3.8 Pa under 50 sccm of argon flow. Pt₃Y and Pt films were 27 nm thick on glassy carbon and 60 nm on GDL, respectively.

2.3 SRPES at Materials Science Beamline of the Elettra Synchrotron

The SRPES measurements were carried out at the Materials Science Beamline (MSB) at the Elettra synchrotron light source in Trieste on an ultra-high vacuum (UHV) end-station with a base pressure below 5×10^{-8} Pa. With a bending magnet source, the MSB provides synchrotron light of a high intensity in the energy range of 21–1,000 eV. The beam size was 0.2×0.8 mm^2. The UHV experimental chamber is equipped with a hemispherical electron energy analyzer (Specs Phoibos 150). Pt₃Y on glassy carbon was measured in the SRPES before acid treatment (as-deposited) and post acid treatment (after immersion in $HClO_4$ acid 3 times for 10 min). The spectra of interest were Pt 4f, Y 3d, O 1s, and C 1s acquired with photon energies of 250, 410, 650, and 990 eV. The total spectral resolutions were about 200 meV (hv = 250 eV), 410 meV (hv = 410 eV), 650 meV (hv = 650 eV), and 1 eV (hv = 990 eV).

To probe a little deeper into the surface, Ar$^+$ sputtering was used to remove the first few layers of material on the surface of the acid treated Pt₃Y sample *in situ*. This included any adventious carbon from ambient air. Ar$^+$ sputtering was performed for 30 seconds at 1 keV energy and 2×10^{-4} Pa pressure, and then again for 10 minutes to probe deeper into and past the overlayer. Spectra were taken after each sputter clean.

Spectra were fitted using KolXPD software. Before fitting, each spectrum was charge corrected using the Fermi edge. A Shirley background was used to fit all the data. In case of the core level Pt 4f spectra fitting procedure the doublet separation for Pt 4f doublet components was set to 3.33 eV and the area ratio to 1.33 [17, 18], the energy position of the $4f_{7/2}$ peak was constrained to be between 70 eV and 71.2 eV. The Lorentzian width was set to 0.4 plus the Fermi edge width for that photon energy [19], the Gaussian width contribution was fixed to the Fermi edge width for 250 eV and 410 eV only. The metallic component of Pt 4f was fit using a Donaich-Šunjić lineshape setting the asymmetry to 0.19 [20]. The asymmetry contribution for the adsorbed C–O component was allowed to vary from 0 to 0.19 and the oxide component was fit with a Voigt line shape with no asymmetry.

The core level Y 3d spectra were fitted with Voigt lineshapes with a doublet split of 2.1 eV and peak ratio of 1.5 [21]. The Lorentzian and Gaussian line widths were kept equal for all components. The metallic peak ($3d_{5/2}$) was constrained to be between 155.9 eV and 156.2 eV, and the oxide between 158 eV and 158.3 eV. Substochiometric oxide was set to vary around 157 eV.

3 Results and Discussion

3.1 Electrochemical Characterization

The behavior of sputtered Pt and Pt₃Y catalyst layers was investigated in a real fuel cell, as the cathode, to provide a practical picture of their activity for ORR. The result is shown in Figure 1. All measurements were taken after treatment in perchloric acid, which induces formation of a Pt overlayer in Pt₃Y. The resultant current densities are normalized to the ECSA and are consistent with our previous measurements by Lindahl et al., whom produced Pt₃Y catalysts using a composite clip target as opposed to an alloy target during sputter deposition [6].

It should be mentioned that there are some difficulties when comparing activities to literature and previous measurements. It can be tricky to assemble laboratory fuel cells in a consistent manner each time. There could be impurities, such as oxygen and carbonates on and within the surface of the catalyst films that alter the activity of the Pt₃Y catalyst. Yttrium is known to react very easily with oxygen, so it is possible that even the smallest amount present during the sputter deposition process could alter the films behavior. Therefore, care must be taken when performing comparisons. However, in this case the result shown is consistent with our previous measurements, indicating that we have reproducibility. Pt₃Y catalyst films have an increase in activity compared to pure Pt. The increase corresponds to the removal of yttrium oxide in acid and the subsequent formation of a highly active Pt overlayer [1, 5, 7, 8, 11], which will be confirmed in the next section.

3.2 SRPES Experiment Results

Spectra were taken of 27 nm of Pt₃Y magnetron sputtered onto glassy carbon disks (i) before acid treatment, (ii) after acid treatment, (iii) after 30 s of Ar$^+$ sputter cleaning, and (iv) 10 min of argon sputter cleaning. Comparing the spectra before and after acid treatment provides information about how the overlayer formed and the effect of ambient air on the quality of the surface. Spectra taken after Ar$^+$ sputtering away the very top layer *in situ*, after acid treatment, shows alloy composition and quality deeper into the surface, revealing factors that can affect the materials activity. The results section will first address the effect of acid treatment on the Pt 4f and Y 3d signal followed by changes due to Ar$^+$ sputtering cleaning of the overlayer.

The Pt 4f spectra taken before and after acid treatment are shown in Figure 2. At each incoming photon energy, the spectra are dominated by a doublet that corresponds to the binding energy of metallic platinum at 71 eV ($4f_{7/2}$) [22–24]. This
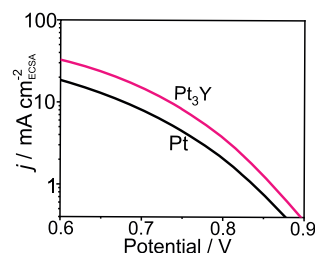

Fig. 1 The electrochemical characterization of a Pt₃Y film sputtered from an alloy target onto GDL. Here Pt₃Y is 2 times more active than sputtered Pt at 0.7 V.
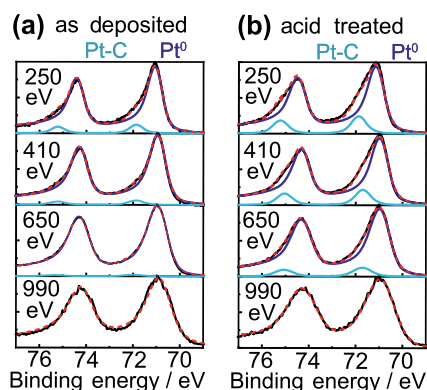
(a) as deposited   **(b)** acid treated

Fig. 2 The Pt 4f core level measured before acid treatment (a) and after (b). The signals have been normalized to the same height. Metallic bulk Pt^0 (dark blue) has a binding energy of 71 eV. A second peak doublet (light blue) has an energy of 71.8 eV and corresponds to adsorbed adventious carbon. The red dotted line is the fit to the data from the two doublets. For 990 eV the only doublet contributing to the fit is Pt^0, so only the fit is shown as they overlap. Acid treatment does not affect the binding of Pt in the alloy. There is, however, an increase in signal amplitude by a factor of 2 after acid treatment, although this is not clear in the figure due to normalization (see Figure 5 for peak signal comparison).
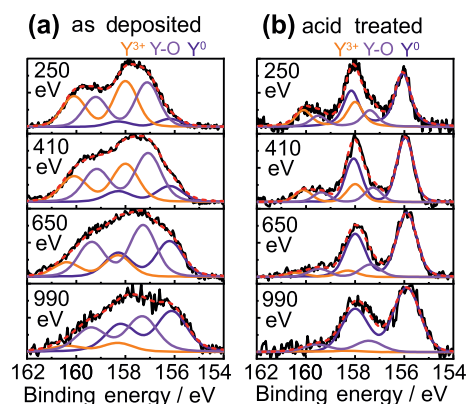

(a) as deposited   **(b)** acid treated

Fig. 3 The effect of acid treatment on Pt₃Y supported on glassy carbon observed through the Y 3d core level. Before treatment (a), there are contributions from metallic yttrium (dark purple line) Y^0 at 155.9 eV, Y₂O₃ (orange line) at 158 eV and substochiometric oxide Y–O (light purple line) around 157 eV. The red dotted line is the fit to the data from the three doublets. The Y^0 contribution increases with increasing photon energy as the Y₂O₃ signal decreases. There is less oxide deeper into the surface, and more metallic yttrium. With acid treatment (b), The Y₂O₃ and Y–O contributions are much less compared to Y^0 as much of the oxide is removed by the acid. The overall signal is much lower here although this is not shown in the figure due to normalization of each spectrum (see Figure 5 for peak signal comparison). Complete oxide removal could require longer acid treatment times, or it could be unreachable by acid, sterically locked in the surface.

value is slightly lower than expected for pure Pt^0 which is caused by alloying with Y. There is a small contribution to the signal at 71.8 eV (Pt–C) on platinum which is likely from an adsorbate possibly due to adventious carbon. The 71.8 eV peak is lower in intensity at higher photon energies as the SRPES collects more bulk Pt^0 photoelectrons which come from deeper within the surface. There is nearly double the intensity from the Pt 4f core level after acid treatment which is not clear on these graphs due to normalization. This is due to the formation of the Pt overlayer (see Figure 5 for comparison of peak intensities and overall alloy content). There are still adsorbates, or substochiometric oxides on the surface after acid treatment, as it was performed in ambient conditions.

Clear trends with photon energy and acid treatment are seen in the Y 3d core levels in Figure 3. For both samples (as-deposited and after acid treatment) there are three contributions to the overall signal: bulk metallic yttrium (Y^0) around 155.9 eV (3d$_{5/2}$), yttrium oxide (Y^{3+}) around 158 eV [21, 25–31]. There is a third peak that we assign to substochiometric Pt₃Y oxide (Y–O) around 157 eV; where the material composition and oxidation is different to Y₂O₃ [14, 32]. There are notable trends with photon energy for all core levels. The contribution of the metallic state (Y^0) increases with higher photon energy. More electrons from the pure alloy, deeper into the surface are collected. The increase in the metallic yttrium peak is accompanied by a decrease in Y₂O₃ signal, indicating that Y₂O₃ is restricted to the surface. There is also a slight decrease in substochiometric oxide, although it is not as drastic as the decrease in Y₂O₃. The Y–O oxide layer gives almost the same signal intensity as Y^0 so there is a similar proportion of them in the material measured at 990 eV. Substochiometric oxide penetrates deeper into the sample than pure yttrium oxide.

Acid treatment significantly reduces the signal contribution from Y₂O₃ as much of it is removed from the top layers,

shown in Figure 3b, in agreement with our previous work and literature [1, 4, 5, 8, 31, 33, 34]. There is still a low contribution from Y₂O₃ and Y–O in the low photon energies, as the acid treatment did not remove all of the surface oxide. Some could be sterically locked inside the alloy. Any remaining non-metallic materials are restricted to the very surface of the sample as there is very little Y₂O₃ and Y–O present at 990 eV. Complete oxide removal could require longer acid treatment times, or it could be unreachable by acid, sterically locked in the surface.

Sputtering away the surface layers of the acid treated sample using Ar$^+$ ions removed any remaining Y₂O₃ and adsorbed carbon, shown in Figure 4. Argon sputtering was performed for 30 seconds and then for another 10 minutes to detect if there were any additional changes to the surface. The Pt 4f spectra, Figure 4a, are only comprised of metallic bulk platinum at 71 eV (4f$_{7/2}$), the adsorbed CO is removed by Ar$^+$ sputter cleaning. The Y 3d core level spectra show the presence of metallic and substochiometric oxide, the Y–O peak is much larger in respect to Y^0 than in Figure 3b, before the sputtering was performed. When sputter cleaning the surface, material from the surface can be pushed further inside, known as forward knock-on sputtering [35]. It is possible that oxygen could be pushed into the alloy increasing the amount of Y–O in this case. The Y–O peak reduces in size when probing with higher photon energies, accompanied by an increase in the metallic peak as electrons are collected from deeper within the alloy. A longer Ar$^+$ sputtering time of 10 min shown in Figure 4c, further increases the contribution from the metallic peak at all energies as more Y–O is removed. The Y–O layer is thick, as it still contributes to the 990 eV excitation after 10 min of

sputtering. However, it is unclear as to how deep the Y–O material is in the film, as the rate of removal of material with sputter cleaning is unknown. The Y–O likely forms during production of the alloy film, but some extra can form due to knock-on sputtering during Ar⁺ sputter cleaning.

The fact that such a large amount of Y–O remains after acid treatment and sputter cleaning shows that this is most likely an oxide peak, as opposed to a Y–C peak found at similar values when using chemical synthesis and carbon supports [32, 36]. There is no carbon present during the film deposition and as yttrium is so oxyphilic, the presence of a very small amount of oxygen in the chamber (during deposition, or from sputter cleaning) could cause substochiometric oxide to form. Previously, we have performed calculations based on this which have shown that subsurface oxygen (which we call substochiometric oxide) will have a shift towards slightly higher binding energies, the sputter cleaning presented in this paper provides further evidence of the existence of subsurface and substochiometric oxide [14]. The percent content of Y^0 to Y–O, showing the distribution at different photon energies, can be found in the supplementary information.

More generally, there are common phenomena for all spectra (Figures 2–4) which can be seen in the peak fits. As both as-deposited and acid treated samples were left in ambient conditions there are many types of surface adsorbates that would have contributed to spectra, which would be particular evident at low energies. These would have been comprised of oxygen, carbon and hydrocarbons, hence why the bulk metallic peaks appear to shift slightly to higher binding energies (0.1–0.2 eV) at low photon energies in both the Pt 4f and Y 3d core level. The instrument and fitting error can also be similar to this value, especially for noisy and low amplitude signals such as the Y 3d spectra presented in this paper. To remove low photon energy bulk peak shifting, the spectra could have

been fit using additional peaks for the varieties of surface adsorbed species present, however this is not a simple task as there could have been many. Additionally, the resolution of the instrument limits the ability to resolve a 0.1 eV peak shift reliably. Only the doublet with 71.8 eV binding energy in the Pt 4f spectra was fit, as the intensity and peak position of the signal was large and discernible enough.

Overall, acid treatment of the Pt₃Y layer decreases the amount of yttrium at the surface of the alloy, shown in Figures 5a and 5b. Before acid treatment, in (a), the alloy is around 75:25 Pt:Y composition as expected from the stoichiometry of Pt₃Y. After acid treatment, in (b), the amount of yttrium (in all forms) is reduced to 4–9% depending on the photon energy. This fact induces the hypothesis that all Y species are buried under a thin overlayer of platinum, as at the lowest photon energy still some Y 3d signal is measured. The mean free path (MFP) for photoelectrons in Pt₃Y at 250 eV is 5.80 Å and in Pt it is 4.99 Å as calculated using TPP-2M formula [37]. So, the platinum overlayer can have a thickness of 1–3 monolayers. A table of the MFP's in Pt and Pt₃Y for each photon energy is shown in the Supporting Information. Using the same formula, it is possible to find the thickness of the yttrium oxide layer on the as-deposited Pt₃Y film. It can be more than 20 Å thick assuming the film is made of mostly Y_2O_3 at the surface. Thus, the presence of yttrium oxide or, on other hand, the Pt overlayer and its thickness could affect the activity of Pt₃Y catalyst. Acid treatment time and vacuum quality, could therefore be important factors in optimizing Pt₃Y catalyst films. It might be useful to plasma clean any PtY catalyst to ensure complete removal of Y_2O_3 near the surface.

After sputter cleaning the amount of yttrium measured increases as adsorbates are removed from the surface. The per-
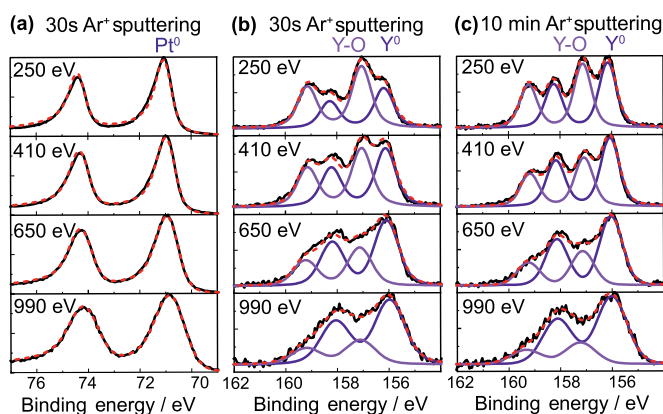

Fig. 4 (a) and (b) show the effect of 30 s of Ar⁺ sputtering on Pt₃Y observed through the Pt 4f (a) and Y 3d core levels, respectively. Argon sputtering for 30 s removes the 71.8 eV peak doublet on Pt (see Figure 2). The red dotted line is the fit to the data, only Pt⁰ is contributing so only the fit is shown (the fit and Pt⁰ doublet overlap). The spectra are unchanged after 10 min of sputter cleaning so, only Pt 4f spectra after 30 s of Ar⁺ sputtering are shown. Ar⁺ sputter cleaning removes all remaining Y₂O₃ from the surface shown in Y 3d spectra (b); (c) shows the effect of 10 min of Ar⁺ sputtering cleaning on the Y 3d core level.
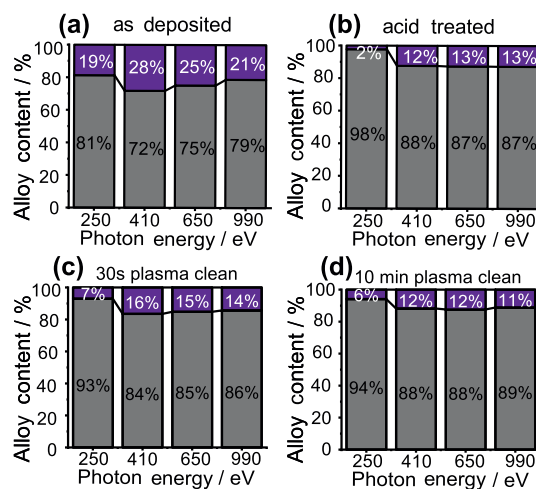

Fig. 5 The ratio of Pt 4f (gray) and Y 3d (purple) core level areas, providing an idea of the alloy composition. Before acid treatment (a) the surface has approximately the stoichiometry for Pt₃Y. Acid treatment (b) decreases the yttrium signal as yttrium oxide is removed from the surface and the overlayer is formed. Ar⁺ sputter cleaning for 30 s (c) removes all remaining Y₂O₃, the amount of Y–O increases with respect to Y⁰. A further 10 min of sputter cleaning causes a reduction in the amount of Y–O measured. This is likely due to a combination of overlayer etching and forward sputtering of oxygen.

ORIGINAL RESEARCH PAPER

centage of Pt 4f to Y 3d is shown Figures 5c and 5d. To compare it is useful to look back at the Y 3d core levels in Figure 4, which shows that there is more Y–O present after 30 s of sputter cleaning, which could be due to forward sputtering of oxygen (Supporting Information Figure S7 shows the ratio of Y:Y–O). However, after 10 min of sputter cleaning the amount of yttrium measured decreases, particularly the Y–O. It could be that initial plasma cleaning pushes oxygen into the film whilst etching away surface adsorbates and the Pt overlayer slightly.

Coming back to the catalyst activity shown in Figure 1, it is clear that the activity increase compared to pure Pt does not match rotating disk electrode measurements reported in literature [5, 7]. There are very well-known reasons for this, RDE is a very optimized measurement. In order to reach higher activities for sputtered films in a fuel cell, the material itself must be optimized, as in [7]. A factor to consider is the morphology of the GDL, but the presence of surface adsorbates and substochiometric oxide in the alloy surface could also affect the activity and will be an important factor with thinner films and nanoparticles as the entire catalyst material may contain oxygen. This shows that there is room for further improvement. Additional examination into the origin of the substochiometric oxide would help improve the application of this catalyst in PEMFC.

4 Conclusions

Magnetron sputtered Pt₃Y catalyst thin films have been shown to provide a significant increase in activity for ORR compared to sputtered platinum. There was twice the specific current, compared to platinum, in fuel cell measurement. SRPES was performed to investigate the quality of the magnetron sputter coating procedure and possibility of surface species reducing the catalytic effect of the films. The technique provided a depth profile for the alloy and overlayer. The 157 eV ($3d_{5/2}$) peak doublet in the Y 3d core level spectra corresponds to a substochiometric oxide. The improved sensitivity of the synchrotron measurements presented here has allowed for its assignment. Although the Y–O layer is thick, much is removed with acid treatment. Slightly sputtering away the surface with Ar⁺ ions does not reduce its contribution to the Y 3d core level by much. Although this seems to indicate that the Y–O could be present throughout the alloy, it is very possible that Ar⁺ sputter cleaning has pushed oxygen further into the alloy surface. This effect provides further evidence that the 157 eV peak is linked to oxygen. Regardless, it is important to use highest vacuum achievable to remove all oxygen that could go into the film when producing the alloy. For the best activity it is important to ensure total removal of Y₂O₃ and Y–O from the surface. This is not the case for the Pt₃Y film presented in this paper. Optimisation of the acid treatment time is also required. Performing acid treatment *in situ*, after sputter deposition of the catalyst film, would elucidate the origin of the substochiometric oxide to aid further improvement of the catalyst performance.

References

[1] M. Escudero-Escribano, P. Malacrida, H. M. Hansen, U. Vej-Hansen, A. Velazquez-Palenzuela, V. Tripkovic, J. Schiøtz, J. Rossmeisl, I. E. L. Stephens, I. Chorkendorff, *Science* **2016**, *352*, 73.

[2] I. E. L. Stephens, J. Rossmeisl, I. Chorkendorff, *Science* **2016**, *354*, 1378.

[3] M. Escudero-Escribano, A. Verdaguer-Casadevall, P. Malacrida, U. Grønbjerg, B. P. Knudsen, A. K. Jepsen, J. Rossmeisl, I. E. L. Stephens, I. Chorkendor, *J. Am. Chem. Soc.* **2012**, *134*, 16476.

[4] J. Greeley, I. E. L. Stephens, A. S. Bondarenko, T. P. Johansson, H. A. Hansen, T. F. Jaramillo, J. Rossmeisl, I. Chorkendorff, J. K. Nørskov, *Nat. Chem.* **2009**, *1*, 552.

[5] N. Lindahl, E. Zamburlini, L. Feng, H. Grönbeck, M. Escudero-Escribano, I. E. L. Stephens, I. Chorkendorff, C. Langhammer, B. Wickman, *Adv. Mater. Interfaces* **2017**, *4*, 1700311.

[6] N. Lindahl, B. Eriksson, H. Grönbeck, R. W. Lindström, G. Lindbergh, C. Lagergren, B. Wickman, *ChemSusChem.* **2018**, *11*, 1438.

[7] S. J. Yoo, K. Lee, S. J. Hwang, Y. Cho, S. Kim, J. W. Yun, Y. Sung, T. Lim, *Int. J. Hydrogen Energy* **2012**, *37*, 9758.

[8] I. E. L. Stephens, A. S. Bondarenko, U. Grønbjerg, J. Rossmeisl, I. Chorkendorff, *Energy Environ. Sci.* **2012**, *5*, 6744.

[9] T. P. Johansson, E. T. Ulrikkeholm, P. Hernandez-Fernandez, M. Escudero-Escribano, P. Malacrida, I. E. L. Stephens, I. Chorkendorff, *Phys. Chem. Chem. Phys.* **2014**, *16*, 13718.

[10] E. Zamburlini, K. D. Jensen, I. E. L. Stephens, I. Chorkendorff, M. Escudero-Escribano, *Electrochim. Acta.* **2017**, *247*, 708.

[11] M. Escudero-Escribano, K. D. Jensen, A. W. Jensen, *Curr. Opin. Electrochem.* **2018**, *8*, 135.

[12] V. R. Stamenkovic, B. S. Mun, K. J. J. Mayrhofer, P. N. Ross, N. M. Markovic, *J. Am. Chem. Soc.* **2006**, *128*, 8813.

[13] I. E. L. Stephens, A. S. Bondarenko, L. Bech, I. Chorkendorff, *ChemCatChem* **2012**, *4*, 341.

[14] R. Brown, M. Vorokhta, I. Khalakhan, M. Dopita, T. Vonderach, T. Skála, N. Lindahl, I. Matolínová, H. Grönbeck, K. M. Neyman, V. Matolín, B. Wickman, *ACS Appl. Mater. Interfaces* **2020**, *12*, 4454.

[15] H. Ekström, P. Hanarp, M. Gustavsson, E. Fridell, A. Lundblad, G. Lindbergh, *J. Electrochem. Soc.* **2006**, *153*, A724.

[16] J. Ihonen, M. Mikkola, G. Lindbergh, *J. Electrochem. Soc.* **2004**, *151*, A1152.

[17] A. Ostroverkh, M. Dubau, V. Johánek, M. Václavů, B. Šmíd, K. Veltruská, Y. Ostroverkh, R. Fiala, V. Matolín, *Fuel Cells* **2018**, *18*, 51.

[18] J. Moulder, W. Stickle, P. Sobol, K. Bomben, *Handbook of X-ray Photoelectron Spectroscopy*, Perkin-Elmer Corp., Physical Electronics Division, Eden Prairie, Minnesota, USA, **1992**.

[19] J. L. Campbell, T. Papp, *At. Data Nucl. Data Tables* **2001**, *77*, 1.

[20] S. Hufner, G. K. Wertheim, *Phys. Rev. B.* **1975**, *11*, 678.

[21] T. Gougousi, Z. Chen, *Thin Solid Films* **2008**, *516*, 6197.

[22] Y. S. Kim, A. Bostwick, E. Rotenberg, P. N. Ross, S. C. Hong, B. S. Mun, *J. Chem. Phys.* **2010**, *133*, 1.

[23] C. Puglia, A. Nilsson, B. Hernnäs, O. Karis, P. Bennich, N. Mårtensson, *Surf. Sci.* **1995**, *342*, 119.

[24] D. J. Miller, H. Øberg, S. Kaya, H. Sanchez Casalongue, D. Friebel, T. Anniyev, H. Ogasawara, H. Bluhm, L. G. M. Pettersson, A. Nilsson, *Phys. Rev. Lett.* **2011**, *107*, 195502.

[25] C. Roy, B. P. Knudsen, C. M. Pedersen, A. Velázquez-Palenzuela, L. H. Christensen, C. D. Damsgaard, I. E. L. Stephens, I. Chorkendorff, *ACS Catal.* **2018**, *8*, 2071.

[26] R. Cui, L. Mei, G. Han, J. Chen, G. Zhang, Y. Quan, N. Gu, L. Zhang, Y. Fang, B. Qian, X. Jiang, Z. Han, *Sci. Rep.* **2017**, *7*, 41826.

[27] M. Tsuji, K. Uto, T. Nagami, A. Muto, H. Fukushima, J. I. Hayashi, *ChemCatChem* **2017**, *9*, 962.

[28] J. S. Kanady, P. Leidinger, A. Haas, S. Titlbach, S. Schunk, K. Schierle-Arndt, E. J. Crumlin, C. H. Wu, A. P. Alivisatos, *J. Am. Chem. Soc.* **2017**, *139*, 5672.

[29] R. Reichl, K. H. Gaukler, *Appl. Surf. Sci.* **1986**, *26*, 196.

[30] T.-M. Pan, J.-D. Lee, *J. Electrochem. Soc.* **2007**, *154*, H698.

[31] P. Malacrida, H. G. Sanchez Casalongue, F. Masini, S. Kaya, P. Hernández-Fernández, D. Deiana, H. Ogasawara, I. E. L. Stephens, A. Nilsson, I. Chorkendorff, *Phys. Chem. Chem. Phys.* **2015**, *17*, 28121.

[32] P. Hernandez-Fernandez, F. Masini, D. N. McCarthy, C. E. Strebel, D. Friebel, D. Deiana, P. Malacrida, A. Nierhoff, A. Bodin, A. M. Wise, J. H. Nielsen, T. W. Hansen, A. Nilsson, I. E. L. Stephens, I. Chorkendorff, *Nat. Chem.* **2014**, *6*, 732.

[33] V. R. Stamenkovic, B. S. Mun, M. Arenz, K. J. J. Mayrhofer, C. A. Lucas, G. Wang, P. N. Ross, N. M. Markovic, *Nat. Mater.* **2007**, *6*, 241.

[34] P. Strasser, S. Koh, T. Anniyev, J. Greeley, K. More, C. Yu, Z. Liu, S. Kaya, D. Nordlund, H. Ogasawara, M. F. Toney, A. Nilsson, *Nat. Chem.* **2010**, *2*, 454.

[35] G. Ceccone, D. Gilliand, W. Kulisch in *Nanotechnological Basis for Advanced Sensors*, Springer Netherlands, Dordrecht, **2011**, p. 99.

[36] R. Brandiele, C. Durante, E. Gradzka, G. A. Rizzi, J. Zheng, D. Badocco, P. Centomo, P. Pastore, G. Granozzi, A. Gennaro, *J. Mater. Chem. A* **2016**, *4*, 12232.

[37] S. Tanuma, C. J. Powell, *Surf. Interface Anal.* **1993**, *21*, 165.

———————————————